Sensors and Actuators B 227 (2016) 547–553

Contents lists available at ScienceDirect

Sensors and Actuators B: Chemical

journal homepage: www.elsevier.com/locate/snb

Hierarchical nanorod-flowers indium oxide microspheres and their gas sensing properties

Xiumei Xu[a,b], Haijiao Zhang[a], Xiaolong Hu[b], Peng Sun[b], Yongsheng Zhu[a], Chaozheng He[a], Shujin Hou[a], Yanfeng Sun[b], Geyu Lu[b,*]

[a] College of Physics and Electronic Engineering, College of Chemistry and Pharmaceutical Engineering, Nanyang Normal University, Nanyang 473061, China
[b] State Key Laboratory on Integrated Optoelectronics, College of Electronic Science and Engineering, Jilin University, Changchun 130012, China

ARTICLE INFO

Article history:
Received 2 June 2015
Received in revised form 27 October 2015
Accepted 26 December 2015
Available online 31 December 2015

Keywords:
In_2O_3
Microspheres
NO_2
Gas sensor

ABSTRACT

In this work, In_2O_3 microspheres with hierarchical nanostructures were successfully synthesized by solvothermal method in the presence of oleic acid and urea. The as-synthesized samples were characterized by X-ray powder diffraction (XRD), field emission scanning electron microscopy (FESEM), transmission electron microscopy (TEM), and high-resolution transmission electron microscopy (HRTEM). The results indicate that the synthesized hierarchical In_2O_3 consists of irregular nanorods. Moreover, the gas sensing properties of as-prepared In_2O_3 hierarchical microspheres were investigated. It was found that the sensor based on such hierarchical nanostructures exhibited high response and good selectivity to NO_2 at 145 °C.

1. Introduction

With the development of industry and the sharp increase of car ownership, the content of NO_2 gas in atmosphere environment consistently increases. NO_2 as a typical air pollutant mainly comes from the exhaust gases of combustion processes, which severely affects the respiratory system of human beings and animals [1–3]. With the growing awareness about environmental pollution and occupational safety issues over the recent decades, how to make high performance and low power consumption sensors for the detection of NO_2 becomes the focus of researchers. Numerous techniques have been developed to detect trace levels of NO_2, such as chemiluminescence, ion chromatography, spectrophotometry, etc. [4–12]. But the cost of existing NO_2 gas detection equipment is high, which is not conducive to its universal access. Therefore, Real-time monitoring and lower-cost sensor is urgently needed for detecting or monitoring ppb-level NO_2 in the atmosphere. Semiconductor gas sensor has become a hot research field because of its high sensitivity, fast response, easy integration, intelligence and enable detection convert sensor integration, etc.

The main component of semiconductor oxide gas sensor is sensitive materials. The key factors influencing the sensitive nature of sensing materials primarily include three aspects: the receptor function, the transducer function and the utility factor of the sensing body [13–16]. Thus, the concepts of sensor design are determined by considering each of these key factors. Based on the above mechanism, we are committed to designing a metal oxide gas sensing material that simultaneously has large specific surface area, good porosity and uniformity. Currently, gas sensitive material for detecting NO_2 are based on ZnO [17], WO_3 [18–20], SnO_2 [21,22], Cu_2O [23], In_2O_3 [24–26], NiO [27] and other composite oxide, but the sensitivity, selectivity and preparation of these materials still cannot meet the requirements. In_2O_3 as a very important n-type semiconductor has been recognized as a promising semiconductor material for gas sensor, window heaters, solar cells, liquid-crystal displays. Among most of the potential applications, the morphology and structure of the nanomaterials will undoubtedly play a pivotal role in determining their properties [28,29]. In order to improve the performance of devices based on In_2O_3, various morphologies of In_2O_3 with different dimensional nanostructures, such as hollow microspheres, nanowires, nanotubes, nanofibers, nanosheets and complex hierarchical structures, have been synthesized via a series of routes, such as vapor-liquid-solid, solution-liquid-solid phase catalytic growth, electrostatic spinning, ultrasonic spray pyrolysis and hydrothermal/solvothermalmethod.

Herein, we report a facile method for the preparation of In_2O_3 nanorod-flowers microspheres by a simple solvothermal process. These diameters of nanorods were about 30–100 nm. Gas-sensing properties of the as-obtained In_2O_3 products were also investigated. The sensor based on the as-obtained In_2O_3 exhibited

* Corresponding author. Tel.: +86 431 851 67808; Fax: +86 431 851 67808.
E-mail address: lugy@jlu.edu.cn (G. Lu).

http://dx.doi.org/10.1016/j.snb.2015.12.085
0925-4005/

Fig 1. Schematic synthesis process of sensing materials.

superior sensing performance to low concentration NO_2 at relatively lower operating temperature.

2. Experimental methods

2.1. Synthesis and characterization of In_2O_3 microspheres

All the reagents (analytical-grade purity) were used without any further purification. In a typical synthesis, 0.381 g of $In(NO_3)_3{\cdot}4.5H_2O$ and 0.25 mL oleic acid were added to 36 mL of water to form a mixed solution. Then 1.0 g of urea was added into the above mixed solution under vigorous stirring. After being stirred and ultrasonically treated alternately, the mixture solution was transferred to a 45 mL teflon-lined stainless steel autoclave, sealed tightly, and maintained at 120 °C for 12 h. After the autoclave was cooled to room temperature naturally, the precipitates were washed with deionized water and absolute ethanol for several times using centrifuge, and then dried at 80 °C for 1 day. The precipitates were loaded into an alumina boat, which was placed in a furnace. For the heat treatment, the samples were calcined at 550 °C for 2 h with a heating rate of 2 °C/min. The calcined products were then collected for further analyses.

X-ray power diffraction (XRD) analysis was conducted on a Rigaku D/max-2500 X-ray diffractometer with Cu Kα1 radiation (λ = 1.54056 Å) in the range of 20–70°. The mean crystallite size was calculated using the Debye-Scherer formula, $D = 0.89\lambda/(\beta\cos\theta)$, where λ is the X-ray wavelength, θ is the Bragg diffraction angle and β is the peak width at half maximum. The specific surface area was estimated using the Brunauer–Emmett–Teller (BET) equation based on the nitrogen adsorption isotherm obtained with a Micromeritics Gemini VII apparatus (Surface Area and Porosity System). Samples were degassed under vacuum at 200 °C for 4 h prior to the measurements. The pore size distribution was determined with the Barrett–Joyner–Halenda (BJH) method applied to the desorption branch of adsorption–desorption isotherm. Field emission scanning electron microscopy (FESEM) images were recorded on a JEOL JSM-7500F microscope operating at 15 kV. Transmission electron microscopy (TEM), selected-area electron diffraction (SAED), and high-resolution transmission electron microscopy (HRTEM) measurements were obtained on a JEOL JEM-2100 microscope operated at 200 kV.

2.2. Fabrication and measurement of sensor

Gas sensors were fabricated as follows: the as-obtained powder was mixed with the deionized water in order to make a paste, which was coated onto an alumina tube (4 mm in length, 1.2 mm in external diameter, and 0.8 mm in internal diameter, attached with a pair of gold electrodes) by a small brush to form a thick film. After drying at room temperature for 24 h, the sensing devices were sintered at 500 °C for 2 h. A pair of gold electrodes was installed at each end of the ceramic tube before it was coated with the paste, and each electrode was connected with two Pt wires. A Ni–Cr heating wire was inserted into the tube to form an indirect-heated gas sensor. Schematic synthesis process of sensing materials is shown in Fig. 1.

The electrical properties of the sensor were measured by CGS-8 intelligent test meter (Beijing Elite Tech. Co., Ltd., China). The response of the sensor was defined as S = Rg/Ra for oxidizing gas or Ra/Rg for reducing gas, here, where Ra and Rg were the resistances of the sensor in the air and target gas, respectively. The response time was defined as the time required for the variation in resistance to reach 90% of the equilibrium value after a test gas was injected, and the recovery time was the time necessary for the sensor to return to 10% above the original resistance in air after releasing the test gas.

3. Results and discussion

3.1. Structural and morphological characteristics of the as-obtained In_2O_3

X-ray powder diffraction (XRD) analysis was performed to investigate the crystal phases of the In_2O_3 products. It can be seen from Fig. 2 that all the diffraction peaks could be very well indexed to the standard cubic In_2O_3, which was consistent with the standard data file (JCPDS file No. 89-4595), with space group Ia-3 (no. 206) and lattice parameters of a = 10.119 Å. The diffraction peaks correspond to (2 1 1), (2 2 2), (4 0 0), (4 1 1), (3 3 2), (1 3 4), (4 4 0), (6 1 1) and (6 2 2), respectively. No diffraction peaks from any other impurities were observed, indicating the high purity of the products.

The morphology of the samples was investigated by field emission scanning electron microscopy (FESEM). Fig. 3 shows typical FESEM images of the sample In_2O_3 at different magnification. The low magnification FESEM image (Fig. 3a) clearly displayed that the products were composed of flower-like microspheres, such microspheres are built from nanorods. No other morphologies can be found in Fig. 3a, which indicated the high uniformity of the as-obtained products. The detailed morphology information about

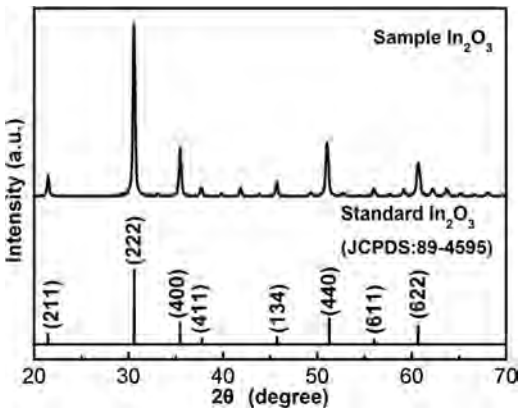

Fig. 2. X-ray diffraction patterns of as-obtained samples.

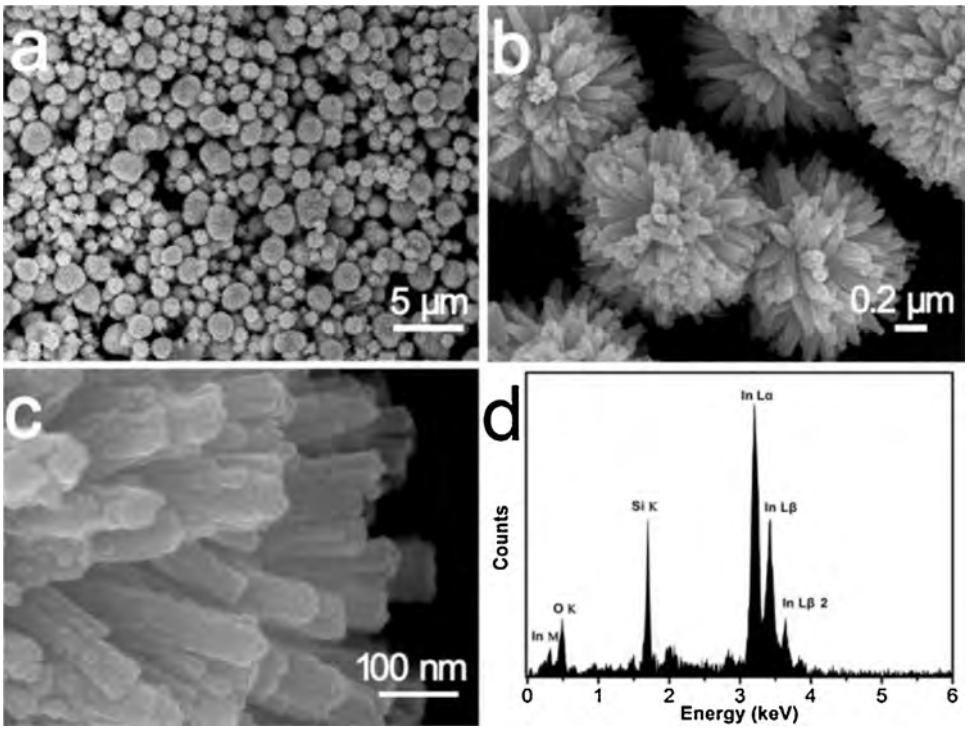

Fig. 3. FESEM images of the as-synthesized In_2O_3: (a) A panoramic and (b) an enlarged of a part of samples. (c) High-magnification FESEM image of In_2O_3 microspheres. (d) EDX pattern of In_2O_3 microspheres.

In_2O_3 was presented in an enlarged-magnification FESEM (Fig. 3b and c), it can be observed that the diameter of the nanorods was about 30–100 nm. The EDX of the products, shown in Fig. 3d, indicates that the obtained In_2O_3 were composed of only three elements: In, O, and Si. (Si from the Si substrate used for SEM measurement).

Further detailed structural analysis of flower-like microspheres was carried out using TEM. Fig. 4a shows the TEM image of representative In_2O_3 microspheres. It can be seen that the size and shape of product were similar to those of the FESEM observations. A high-magnification TEM (Fig. 4b) image presents that the diameter of these irregular nanorods was about 30–100 nm. The selected-area electron diffraction (SAED) pattern of an individual In_2O_3 nanorod (Fig. 4c) confirms that the as-synthesized products were polycrystalline in structure. The high-resolution transmission electron microscopy (HRTEM) image (Fig. 4d) showed fringe distance of 0.292 nm, corresponding to the lattice distances of the (2 2 2) plane of cubic In_2O_3.

To investigate the role of urea in the formation of hierarchical In_2O_3 microspheres, the controlled experiments of the solvothermal process with different concentrations of urea had been carried out by keeping other experimental conditions constant. When the experiments were performed with adding 0.1 g urea, only nanocubes were obtained (Fig. 5a). As shown in Fig. 5b, upon adding 0.3 g of urea, the obtained products consisted of nanoplates. As shown in Fig. 5c, upon adding 1.0 g of urea, the obtained products consisted of regular hierarchical In_2O_3 microspheres. According to the above results, it can be concluded that urea may play ternary roles including being the alkaline media, the coordinating agent and the surface anchored organic molecules [26,30,31].

To further obtain the information about the as-prepared In_2O_3 hierarchical microspheres, the nitrogen adsorption and desorption measurements were performed at 77 K. The nitrogen adsorption–desorption isotherms and the corresponding BJH pore size distribution plot (inset of Fig. 6) of the hierarchical microspheres were shown in Fig. 6. The adsorption–desorption isotherms were typical type IV with a hysteresis loop according to the IUPAC classification, indicating that the powders contain disordered pores. Pore size distribution curves were calculated from the desorption branch of a nitrogen isotherm by the BJH method using

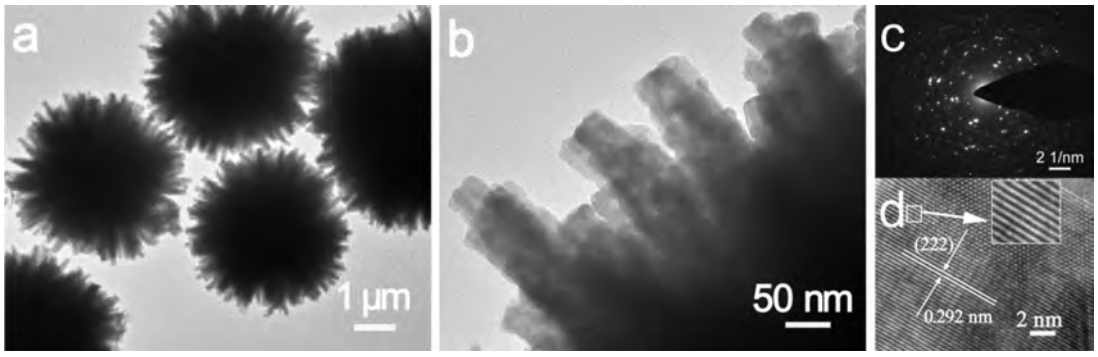

Fig. 4. Typical TEM images (a and b) of In_2O_3 nanostructures. (c) The corresponding SAED pattern. (d) HRTEM images taken from (a and b).

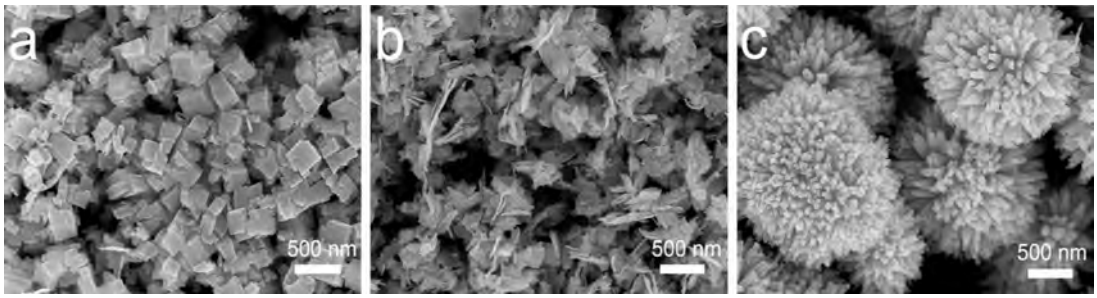

Fig. 5. FESEM images of In_2O_3 products synthesized under hydrothermal reaction with the presence of different amounts of urea of (a) 0.1 g, (b) 0.3 g and (c) 1.0 g, respectively.

the Halsey equation. The BET surface area of the product was calculated to be 35.4 m^2/g with the Brunauer–Emmett–Teller (BET) method.

3.2. Gas-sensing properties for NO_2

In order to determine an optimum operating temperature, the response of the sensor toward 1 ppm NO_2 was examined as a function of operating temperature [14,15,32,33]. The correlations of the response and response time of the sensor based on flower-like In_2O_3 microspheres to 1 ppm NO_2 with the operating temperature, respectively, were measured and shown in Fig. 7. It is revealed that the response time decreased with increasing operating temperature. This tendency indicates that fast response can be obtained by increasing the operating temperature. For the sensor using the flower-like In_2O_3 microspheres, the response to 1 ppm NO_2 increases when operating temperature varies from 132 to 145 °C. However, when the operating temperature was higher than 145 °C, the response gradually decreases. Accordingly, the optimum operating temperature for the sensor using the as-obtained In_2O_3 was believed to be 145 °C, which was applied in all the investigations hereinafter. A comparison between the sensing performances of the sensor and literature reports is summarized in Table 1. It is noteworthy that the sensor fabricated in our work exhibits better sensing performances compared with those reported in the literature [24,34–42].

The response transients of the flower-like In_2O_3 microspheres sensor to 1 ppm NO_2 was measured at 145 °C (Fig. 8), the response time and recovery time were about 60 s and 30 s, respectively. The five reversible cycles of the response curve indicated the sensor has a stable and repeatable response characteristic, as shown in the inset of Fig. 8. It can be observed that the average response was 132 to 1 ppm NO_2. The dynamic response resistances of the sensors based on In_2O_3 microspheres (Fig. 9) to different NO_2 concentrations were investigated at 145 °C. The resistance of the sensor increases upon exposure of NO_2, whereas it decreases upon the removal of NO_2. Furthermore, the response of the sensor to NO_2 increased with the increasing of the NO_2 concentration. The sensor can detect 1 ppm NO_2, and the response was 132. The responses to 0.2, 0.4, 0.8, 1.0, 1.2, 1.4, 1.8 and 2.0 ppm NO_2 were about 29, 59, 93, 132, 153, 174, 196 and 220, respectively.

The gas sensing is a surface-related phenomenon, which involves the adsorption or desorption of gaseous molecules and the interaction (electronic or chemical) among these different kinds of gas molecules on the surface of sensing film [43–46]. For the semiconductor oxide, the most widely accepted sensing mechanism

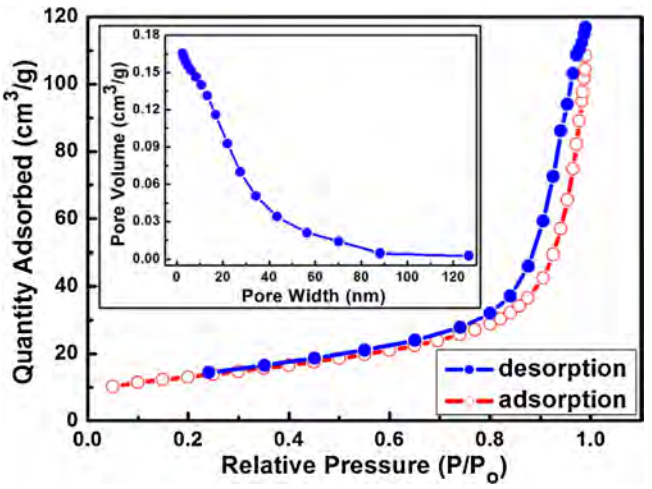

Fig. 6. Nitrogen adsorption-desorption isotherms. The inset is pore size distribution calculated from the adsorption branch of the isotherms.

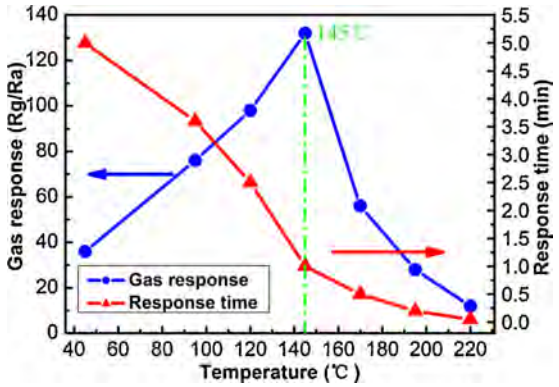

Fig. 7. Correlations between the gas response and response time to 1 ppm NO_2 and the operating temperature for the sensor using the as-obtained In_2O_3.

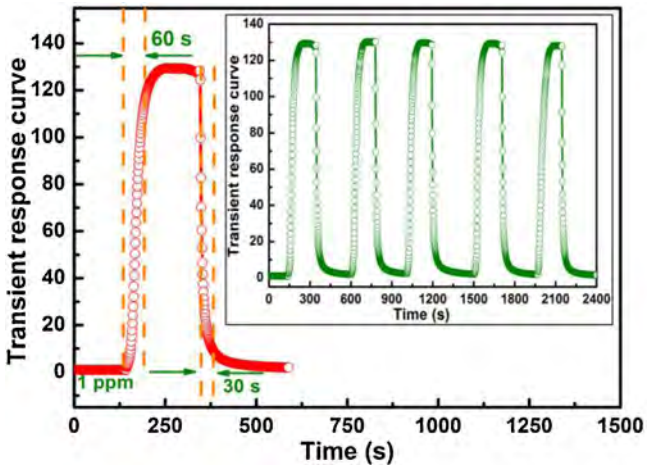

Fig. 8. Response transients curve and the inset is the repeated response transients curves to1 ppm for the sensor NO_2 at 145 °C.

Table 1
Gas responses to NO_2 in the present study and those reported in the literatures [24,34–42].

Materials	NO_2 concentration (ppm)	Operating temperature (°C)	Response (Rg/Ra)	References
Porous rh-In_2O_3 nanosheets	50	250	164	[34]
Nonporous In_2O_3 nanosheets	50	250	57	[34]
Lotus root slicelike In_2O_3 microspheres	50	250	90	[35]
In_2O_3 hollow spheres	100	215	2	[36]
Zn-doped In_2O_3 hollow sphere	50	300	100	[37]
Zn-doped In_2O_3 cubes	50	300	70	[38]
SnO_2 microrods	50	300	<100	[39]
CuO nanosheets	100	240	<10	[40]
In_2O_3 nanowires	1	250	2.57	[24]
In_2O_3 nanofibers	100	300	1.8	[41]
SnO_2-In_2O_3 nanostructures	2	250	125	[42]
Nanorod-flowers In_2O_3 microspheres	1	145	132	This work

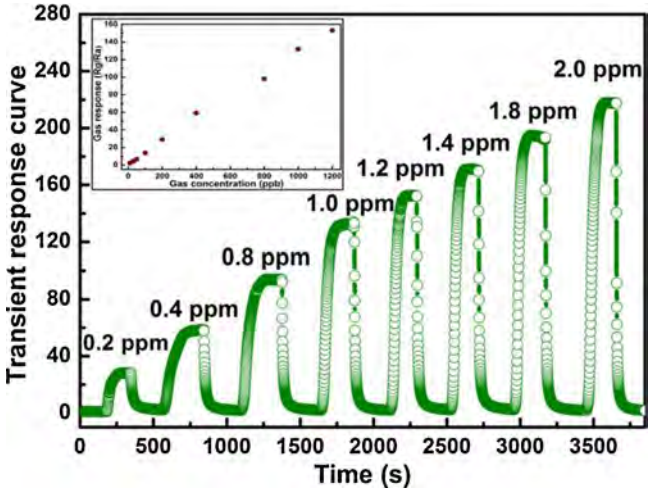

Fig. 9. The dynamic transient response curve of the sensors and the gas responses to different concentrations of NO_2 for the sensor using In_2O_3 microspheres at 145 °C in the range of 0.2–2 ppm.

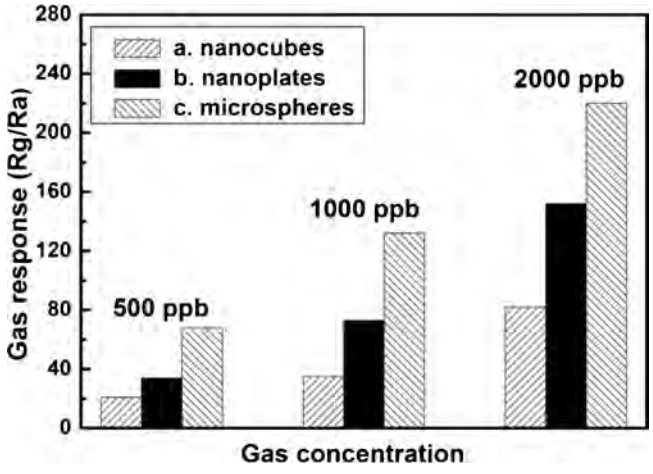

Fig. 10. Responses of sensors based on different nanostructures (a. Nanocubes, b. Nanoplates, c. microspheres) vs different gas concentration.

states that "when the sensor is exposed to air, oxygen molecules are adsorbed on the surface of the sensing materials, and ionized by electrons from the conduction band of materials to form chemisorbed oxygen species." [13–15,47,48]. The ability of the sensing material to absorb and ionize oxygen species is fundamental to the performance of sensor. When the In_2O_3 sensors were exposed to air atmosphere, the grains of In_2O_3 were naturally surrounded by ambient oxygen molecules, which could extract free electrons from the conduction of In_2O_3 causing the formation of chemisorbed oxygen species (O^{2-}, O^- or O_2^-) on the surface [14,15,43,42]. The NO_2 sensing mechanism can be described in two ways: the molecules can be directly adsorbed onto the surface by extracting electrons from the conduction band (Eq. (1)) or they can interact with the chemisorbed oxygen on the surface (Eqs. (2) and (3)) [49–52].

$$NO_{2(gas)} + e- \rightarrow NO_2{}^-{}_{(ads)} \quad (1)$$

$$NO_{2(gas)} + 2O^-{}_{(ads)} \rightarrow NO_2{}^-{}_{(ads)} + O_{2(gas)} + e^- \quad (2)$$

$$NO_{2(gas)} + O^-{}_{(ads)} \rightarrow NO^+{}_{(ads)} + 2O^-{}_{(ads)} \quad (3)$$

The enhancement in gas-sensing property for porous In_2O_3 hierarchical architectures may be ascribed to the abundant framework of gas diffusion and the chemical absorption as well as reaction on the surface of the In_2O_3 [53–55]. In Fig. 10, the hierarchical In_2O_3 microspheres showed significantly enhanced response to NO_2 compared with nanocubes (Fig. 5a) or nanoplates (Fig. 5b). There exists a network of interconnected pores in sensing layer of the In_2O_3 sensor, where the diffusion of target gas toward all of the surfaces of In_2O_3 nanorods was effective. Moreover, it has been reported that grain boundaries or grain junctions were considered as the active sites and they act positively on the performance of sensor [47,53,56]. The as-prepared In_2O_3 microspheres were composed of many well-aligned nanorods, and many nanorods/nanorods grain boundaries could be formed. The more detailed reason and qualitative explanation need further investigation.

Selectivity was an important parameter for gas sensor. Fig. 11 shows the cross-sensitivities of the sensor using the In_2O_3 microspheres to various gases, including O_3, H_2S, Cl_2, SO_2, C_2H_5OH,

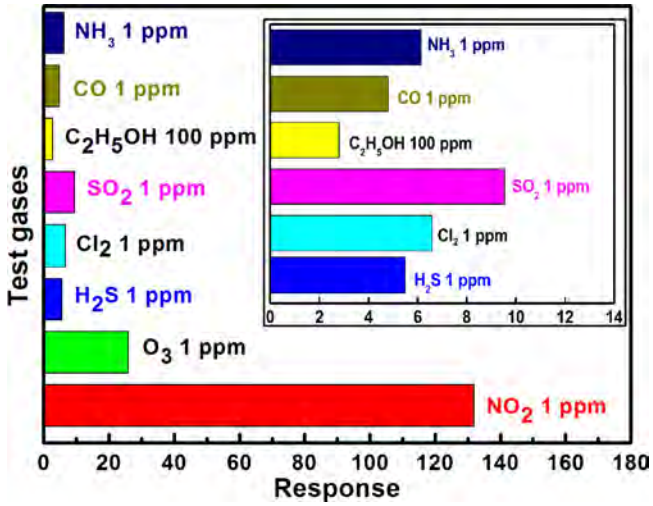

Fig. 11. Cross-responses of In_2O_3 microspheres sensor to various test gases at 145 °C.

CO, and NH_3. It is clear that the In_2O_3 sensor exhibits the largest response to NO_2 among the tested gases. Such a result indicates that the sensor using the In_2O_3 nanostructure exhibits an excellent selectivity to NO_2 against the other tested gases at the operating temperature of 145 °C.

4. Conclusion

In summary, In_2O_3 microspheres had been successfully synthesized through a simple one-step solution route combined with a subsequent calcining process. Field emission scanning electron microscopic and transmission electron microscopic results demonstrate that the diameter of nanorods was about 30–100 nm. The sensor fabricated using these hierarchical structures exhibited excellent NO_2 sensing properties at relatively lower operating temperature. The response of sensor was about 132 to 1 ppm NO_2 at 145 °C. Moreover, the hierarchical In_2O_3 exhibits significantly enhanced response to NO_2 compared with nanocubes or nanoplates.

Acknowledgements

This work is supported by the National Nature Science Foundation of China (No. 61327804, 61473132, 61304242, 61474057, 51501093 and 11504188), Natural Science Foundation of Nanyang Normal University (No.zx2015001, 2015003, 2015006), the Henan Joint Funds of the National Natural Science Foundation of China (No. U1304612, U1404608, U1404216 and U1504626), Program for Chang Jiang Scholars and Innovative Research Team in University (No.IRT13018) and "863" High Technology Project (2013AA030902 and 2014AA06A505).

References

[1] D.H. Zhang, Z.Q. Liu, C. Li, T. Tang, X.L. Liu, S. Han, B. Lei, C.W. Zhou, Detection of NO_2 down to ppb levels using individual and multiple In_2O_3 nanowire devices, Nano Lett. 4 (2004) 1919–1924.
[2] C. Baatto, E. Comini, G. Sberveglieri, M. Jha, A. Zappettini, Metal oxide nanocrystals for gas sensing, Sensor Actuat. B Chem. 109 (2005) 2–6.
[3] U.S. environmental protection agency, Air Trends Summary Report, http://www.epa.go/oar/aqtrnd95/no2.html.
[4] P. Mikuška, Z. Večeřa, Simultaneous determination of nitrite and nitrate in water by chemiluminescent flow-injection analysis, Anal. Chim. Acta 495 (2003) 225–232.
[5] D.A. Day, P.J. Wooldridge, M.B. Dillon, J.A. Thornton, R.C. Cohen, A thermal dissociation laser-induced fluorescence instrument for in situ detection of NO_2, peroxy nitrates, alkyl nitrates, and HNO_3, J. Geophys. Res. Atmos. 107 (2002) 1–14.
[6] R.S. Braman, S.A. Hendrix, Nanogram nitrite and nitrate determination in environmental and biological materials by vanadium (III) reduction with chemiluminescence detection, Anal. Chem. 61 (1989) 2715–2718.
[7] I.B. Pollack, B.M. Lerner, T.B. Ryerson, Evaluation of ultraviolet light-emitting diodes for detection of atmospheric NO_2 by photolysis-chemiluminescence, J. Automat. Chem. 65 (2010) 111–125.
[8] A. Aydm, Ö. Ercan, S. Tascioglu, A novel method for the spectrophotometric determination of nitrite in water, Talanta 66 (2005) 1181–1186.
[9] Z. Vecera, P.K. Dasgupta, Measurement of atmospheric nitric and nitrous acids with a wet effluent diffusion denuder and low-pressure ion chromatography -postcolumn reaction detection, Anal. Chem. 63 (1991) 2210–2216.
[10] J.P. Murrihy, M.C. Breadmore, A. Tan, M. McEnery, J. Alderman, C. O'Mathuna, A.P. O'Neill, P. O'Brien, N. Advoldvic, P.R. Haddad, J.D. Glennon, Ion chromatography on-chip, J. Chromatogr. A 924 (2001) 233–238.
[11] G.M. Greenway, S.J. Haswell, P.H. Petsul, Characterisation of a micro-total analytical system for the determination of nitrite with spectrophotometric detection, Anal. Chim. Acta 387 (1999) 1–10.
[12] J.T. Groves, J.B. Lee, S.S. Marla, Detection and characterization of an oxomanganese (V) porphyrin complex by rapid-mixing stopped-flow spectrophotometry, J. Am. Chem. Soc. 119 (1997) 6269–6273.
[13] S.R. Morrison, Selectivity in semiconductor gas sensors, Sensor Actuat. B Chem. 12 (1987) 425–440.
[14] N. Yamazoe, New approaches for improving semiconductor gas sensor, Sensor Actuat. B Chem. 5 (1991) 7–19.
[15] N. Yamazoe, G. Sakai, K. Shimanoe, Oxide semiconductor gas sensor, Catal. Surv. Asia 7 (2003) 63–75.
[16] M. Egashira, Y. Shimizu, Y. Takao, S. Sako, Variations in I–V characteristics of oxide semiconductors induced by oxidizing gases, Sensor Actuat. B Chem. 35 (1996) 62–67.
[17] C. Baatto, G. Sberveglieri, A. Onischuk, B. Caruso, S. di Stasio, Low temperature selective NO_2 sensors by nanostructured fibres of ZnO, Sensor Actuat. B Chem. 100 (2004) 261–265.
[18] D.S. Lee, S.D. Han, J.S. Huh, D.D. Lee, Nitrogen oxides-sensing characteristics of WO_3-based nanocrystalline thick film gas sensor, Sensor Actuat. B Chem. 60 (1999) 57–63.
[19] S.H. Wang, T.C. Chou, C.C. Liu, Nano-crystalline tungsten oxide NO_2 sensor, Sensor Actuat. B Chem. 94 (2003) 343–351.
[20] C. Zhang, M. Debliquy, A. Boudiba, H. Liao, C. Coddet, Sensing properties of atmospheric plasma-sprayed WO_3 coating for sub-ppm NO_2 detection, Sensor Actuat. B Chem. 144 (2010) 280–288.
[21] J. Zhang, S. Wang, Y. Wang, Y. Wang, B. Zhu, H. Xia, X. Guo, S. Zhang, W. Huang, S. Wu, NO_2 sensing performance of SnO_2 hollow-sphere sensor, Sensor Actuat. B Chem. 135 (2009) 610–617.
[22] L. Li, S. He, M. Liu, C. Zhang, W. Chen, Three-dimensional mesoporous graphene aerogel-supported SnO_2 nanocrystals for high-performance NO_2 gas sensing at low temperature, Anal. Chem. (87) (2015) 1638–1645.
[23] S. Deng, V. Tjoa, H.M. Fan, H.R. Tan, D.C. Sayle, M. Olivo, S. Mhaisalkar, J. Wei, C.H. Sow, Reduced graphene oxide conjugated Cu_2O nanowire mesocrystals for high-performance NO_2 gas sensor, J. Am. Chem. Soc. 134 (2012) 4905–4917.
[24] P.C. Xu, Z.X. Cheng, Q.Y. Pan, J.Q. Xu, Q. Xiang, W.J. Yu, Y.L. Chu, High aspect ratio In2O3 nanowires: synthesis, mechanism and NO_2 gas-sensing properties, Sensor Actuat. B Chem. 130 (2008) 802–808.
[25] M. Ivanovskaya, A. Gurlo, P. Bogdanov, Mechanism of O_3 and NO_2 detection and selectivity of In_2O_3 sensors, Sensor Actuat. B Chem. 77 (2001) 264–267.
[26] Z.Y. He, Z.H. Chen, Y.G. Li, H.Z. Zhang, Wang, Molar ratio of In to urea directed formation of In_2O_3 hierarchical structures: cubes and nanorod-flowers, Cryst. Eng. Commun. 13 (2011) 2557–2565.
[27] V.V. Plashnitsaa, V. Guptab, N. Miurac, Mechanochemical approach for fabrication of a nano-structured NiO-sensing electrode used in a zirconia-based NO_2 sensor, Electrochim. Acta. 55 (2010) 6941–6945.
[28] Y.N. Xia, P.D. Yang, Y.G. Sun, Y.Y. Wu, B. Mayers, B. Gates, Y.D. Yin, F. Kim, Y.Q. Yan, One-dimensional nanostructures: synthesis, characterization, and applications, Adv. Mater. 15 (2003) 353–389.
[29] J.-H. Lee, Gas sensors using hierarchical and hollow oxide nanostructures: overview, Sensor Actuat. B Chem. 140 (2009) 319–336.
[30] H.B. Wu, J.S. Chen, X.W. Lou, H.H. Hng, Synthesis of SnO_2 hierarchical structures assembled from nanosheets and their lithium storage properties, J. Phys. Chem. C 115 (2011) 24605–24610.
[31] X.X. Xu, P.L. Zhao, D.W. Wang, P. Sun, L. You, Y.F. Sun, X.S. Liang, F.M. Liu, H. Chen, G.Y. Lu, Preparation and gas sensing properties of hierarchical flower-like In_2O_3 microspheres, Sensor Actuat. B Chem. 176 (2013) 405–412.
[32] T. Kida, A. Nishiyama, M. Yuasa, K. Shimanoe, N. Yamazoe, Highly sensitive NO_2 sensors using lamellar-structured WO_3 particles prepared by an acidification method, Sensor Actuat. B Chem. 135 (2009) 568–574.
[33] K.I. Choi, H.R. Kim, J.H. Lee, Enhanced CO sensing characteristics of hierarchical and hollow In_2O_3 microspheres, Sensor Actuat. B Chem. 138 (2009) 497–503.
[34] L.P. Gao, Z.X. Cheng, Q. Xiang, Y. Zhang, J.Q. Xu, Porous corundum-type In_2O_3 nanosheets: synthesis and NO_2 sensing properties, Sensor Actuat. B Chem. 208 (2015) 436–443.
[35] Z.X. Cheng, L.Y. Song, X.H. Ren, Q. Zheng, J.Q. Xu, Novel lotus root slice-like self-assembled In_2O_3 microspheres: synthesis and NO_2-sensing properties, Sensor Actuat. B Chem. 176 (2013) 383–389.
[36] T. Zhang, F.B. Gu, D.M. Han, Z.H. Wang, G.S. Guo, Synthesis, characterization and alcohol-sensing properties of rare earth doped In_2O_3 hollow spheres, Sensor Actuat. B Chem. 177 (2013) 1180–1188.
[37] P. Li, H.Q. Fan, Y. Cai, M.M. Xu, Zn-doped In_2O_3 hollow spheres: mild solutionreaction synthesis and enhanced Cl_2 sensing performance, Cryst. Eng. Commun. 16 (2014) 2715–2722.
[38] P. Li, H.Q. Fan, Y. Cai, M.M. Xu, C.B. Long, M.M. Li, S.H. Lei, X.W. Zou, Phase trans-formation (cubic to rhombohedral): the effect on the NO_2 sensing performanceof Zn-doped flower-like In_2O_3 structures, RSC adv. 4 (2014) 15161–15170.
[39] S.W. Choi, A. Katoch, G.J. Sun, P. Wu, S.S. Kim, NO_2-sensing performance of In_2O_3 microrods by functionalization of Ag nanoparticles, J. Mater. Chem. 1 (2013) 2834–2841.
[40] F. Zhang, A.W. Zhu, Y.P. Luo, Y. Tian, J.H. Yang, Y. Qin, CuO nanosheets for sen-sitive and selective determination of H_2S with high recovery ability, J. Phys. Chem. C 114 (2010) 19214–19219.
[41] W. Zheng, X.F. Lu, W. Wang, Z.Y. Li, H.N. Zhang, Y. Wang, Z.J. Wang, C. Wang, A highly sensitive and fast-responding sensor based on electrospun In_2O_3 nanofibers, Sensor Actuat. B Chem. 142 (2009) 61–65.
[42] A. Forleo, L. Francioso, M. Epifani, S. Capone, A.M. Taurino, P. Siciliano, NO_2-gas-sensing properties of mixed In_2O_3-SnO_2 thin films, Thin Solid Films 490 (2005) 68–73.
[43] N. Matsunaga, G. Sakai, K. Shimanoe, N. Yamazoe, Formulation of gas diffusion dynamics for thin film semiconductor gas sensor based on simple reaction-diffusion equation, Sensor Actuat. B Chem. 96 (2003) 226–233.
[44] N. Yamazoe, K. Shimanoe, Theory of power laws for semiconductor gas sensors, Sensor Actuat. B Chem. 128 (2008) 566–573.
[45] N. Yamazoe, K. Shimanoe, Theoretical approach to the rate of response of semiconductor gas sensor, Sensor Actuat. B Chem. 150 (2010) 132–140.

[46] M. Yuasa, T. Kida, K. Shimanoe, Preparation of a stable sol suspension of Pd-loaded SnO_2 nanocrystals by a photochemical deposition method for highly sensitive semiconductor gas sensors, ACS Appl. Mater. Interfaces 4 (2012) 4231–4236.
[47] J. Ding, T.J. McAvoy, R.E. Cavicchi, Semancik, Surface state trapping model for SnO_2-based microhotplate sensors, Sensor Actuat. B Chem. 77 (2001) 597–631.
[48] C.S. Rout, K. Ganesh, A. Govindaraj, C.N.R. Rao, Sensors for the nitrogen oxides, NO_2 NO and N_2O, based on In_2O_3 and WO_3 nanowires, Appl. Phys. A 85 (2006) 241–246.
[49] I. Hwang, S. Kim, J. Choi, J. Choi, H. Ji, G. Kim, G. Cao, J. Lee, Synthesis and gas sensing characteristics of highly crystalline ZnO-SnO_2 core–shell nanowires, Sensor Actuat. B Chem. 148 (2010) 595–600.
[50] N. Barsan, D. Koziej, U. Weimar, Metal oxide-based gas sensor research: How to? Sensor Actuat. B Chem. 121 (2007) 18–35.
[51] L. Francioso, A. Forleo, S. Capone, M. Epifani, A.M. Taurino, P. Siciliano, Nanostructured In_2O_3-SnO_2 sol-gel thin film as material for NO_2 detection, Sensor Actuat. B Chem. 114 (2006) 646–655.
[52] M. Epifani, J.D. Prades, E. Comini, E. Pellicer, M. Avella, P. Siciliano, G. Faglia, A. Cirera, R. Scotti, F. Morazzoni, J.R. Morante, The role of surface oxygen vacancies in the NO_2 sensing properties of SnO_2 nanocrystals, J. Phys. Chem. C 112 (2008) 19540–19546.
[53] E. Li, Z.X. Cheng, J.Q. Xu, Q.Y. Pan, W.J. Yu, Y.L. Chu, Indium oxide with novel morphology: synthesis and application in C_2H_5OH gas sensing, Cryst. Growth Des. 9 (2009) 2146–2151.
[54] P. Sun, W. Zhao, Y. Cao, Y. Guan, Y.F. Sun, G.Y. Lu, Porous SnO_2 hierarchical nanosheets: hydrothermal preparation, growth mechanism, and gas sensing properties, Cryst. Eng. Commun. 13 (2011) 3718–3724.
[55] N. Yamazoe, K. Shimanoe, Roles of shape and size of component crystals in semiconductor gas sensors, J. Electrochem. Soc. 155 (2008) 93–98.
[56] P. Sun, C. Wang, X. Zhou, P.F. Cheng, K. Shimanoe, G.Y. Lu, N. Yamazoe, Cu-doped α-Fe_2O_3 hierarchical microcubes: synthesis and gas sensing properties, Sensor Actuat. B Chem. 193 (2014) 616–622.

Biographies

Xiumei Xu received her BS degree from Liaocheng University of China in 2008 and her PhD degree from Jilin University of China in 2014. Now, she is a lecturer in Nanyang Normal University. She is engaged in the synthesis and characterization of the semiconducting functional materials and gas sensors.

Haijiao Zhang received his BS degree from Liaocheng University of China in 2008 and the MS degree from LiaoNing ShiHua University of China in 2011. Now, he is a teacher in Nanyang normal university.

Xiaolong Hu received his BS degree from the Electronics Science and Engineering Department, Jilin University, China in 2011. Presently, he is a PhD student, majored in microelectronics and solid state electronics. Now, he is engaged in the synthesis and characterization of the semiconducting functional materials and gas sensors.

Peng Sun received his PhD degree from the Electronics Science and Engineering department, Jilin University, China in 2014. Now, he is engaged in the synthesis and characterization of the semiconducting functional materials and gas sensors.

Yongsheng Zhu received his BS degree from Nanyang Normal University of China in 2009 and his PhD degree from Jilin University of China in 2014. His research interests are the modulation of the rare earth ions in inverse opal photonic crystals.

Chaozheng He obtained his BS degree from Changchun Normal University of China in June of 2006 and his PhD degree from Jilin University of China in June of 2013. Since July of 2013, he has worked in Nanyang Normal University, China, as an associate professor. His research interests focus on heterogeneous catalysis, such as structure-activity relationship and mechanisms of catalytic reactions.

Shujin Hou received his BS degree from Nanyang Normal University of China in 2004 and his PhD degree from Xianmen University of China in 2014. Now, he is a lecturer in Nanyang Normal University. He is engaged in theoretical physics.

Yanfeng Sun obtained his PhD from Jilin University of China in 2007. Presently, he is working as associate professor in Electronics Science and Engineering department of Jilin University. His current research interests are nanoscience and gas sensors.

Geyu Lu received his BS degree in electronic sciences in 1985 and his MS degree in 1988 from Jilin University in China and the Dr. Eng. degree in 1998 from Kyushu University in Japan. Now he is a professor of Jilin University, China. Now, he is interested in the development of functional materials and chemical sensors.